Volume 4
Number 12
December 2025
Pages 1405–1542

Energy Advances

rsc.li/energy-advances

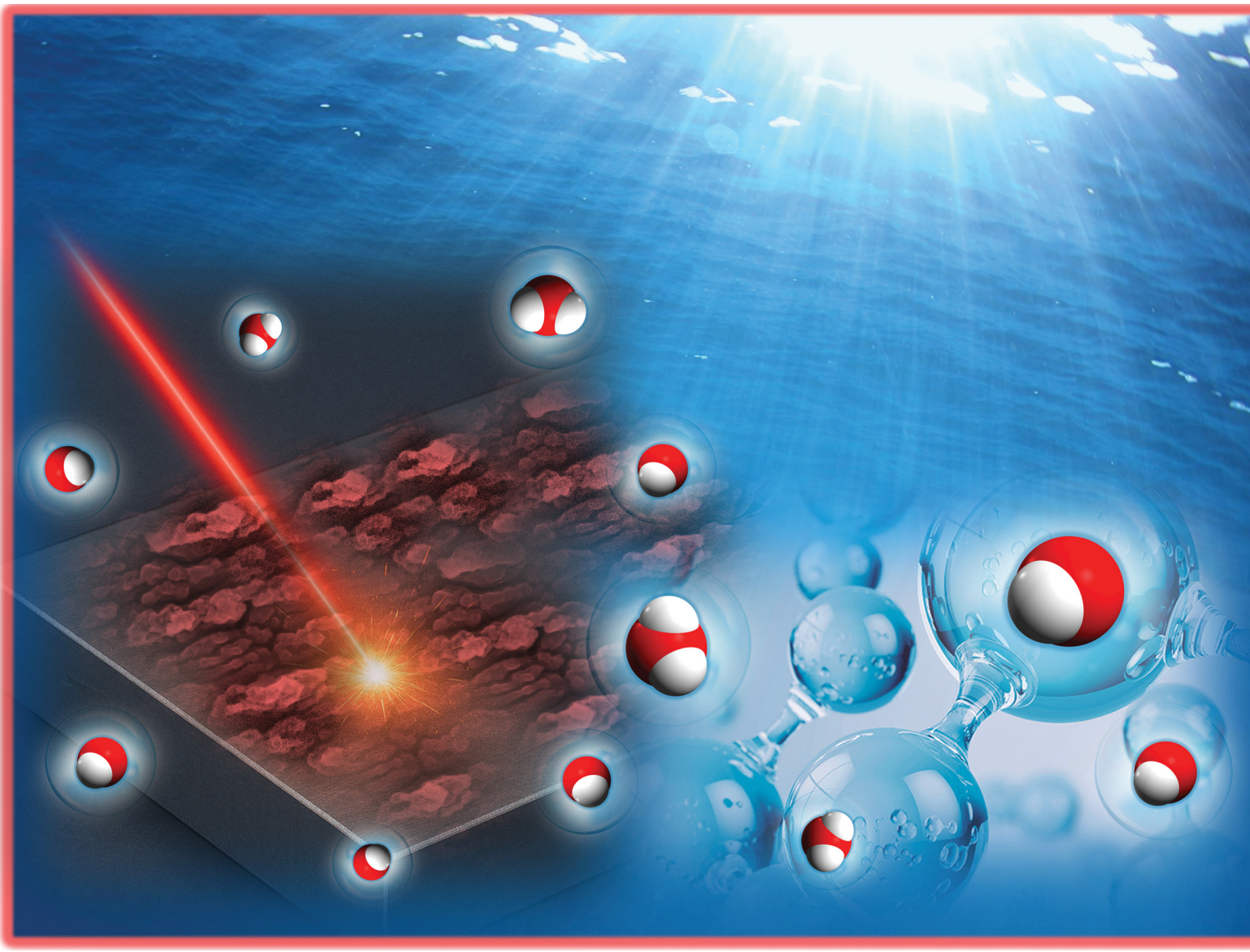

ISSN 2753-1457

ROYAL SOCIETY OF CHEMISTRY

COMMUNICATION

Davide Barreca *et al.*

Enhancing oxygen evolution performances of NiO-based electrocatalysts through synergistic plasma processing and laser treatment

Energy Advances

ROYAL SOCIETY OF CHEMISTRY

COMMUNICATION

View Article Online
View Journal | View Issue

Cite this: *Energy Adv.*, 2025, 4, 1426

Received 15th September 2025,
Accepted 15th October 2025

DOI: 10.1039/d5ya00273g

rsc.li/energy-advances

Enhancing oxygen evolution performances of NiO-based electrocatalysts through synergistic plasma processing and laser treatment

Davide Barreca, *[a] Alessandro Bellucci, [b] Matteo Mastellone, [c] Daniele Maria Trucchi, [b] Chiara Maccato, [ad] Ermanno Pierobon, [d] Alberto Gasparotto [ad] and Gian Andrea Rizzi [ad]

The continuous search for oxygen evolution reaction (OER) electrocatalysts as greener substitutes for noble metal-based ones has spotlighted NiO-based systems as attractive and economically viable candidates, thanks to their affordability and electrochemical virtues. Nevertheless, progresses in this field require additional research efforts aimed at improving material performances, towards their possible real-world applications. In this context, the present work proposes an original processing route to boost OER performances of NiO-based systems, involving plasma-assisted growth followed by ultrafast laser processing under controlled conditions. The activated catalysts featured a significant enhancement in water oxidation performances, corresponding in the best case to a low Tafel slope of ≈40 mV × dec^{-1} and an overpotential of ≈380 mV at 10 mA × cm^{-2}. Overall, these results may provide valuable insights for the development of high-performance electrocatalysts with modular properties.

The quest for sustainable energy sources capable of satisfying the ever-growing planet needs and decarbonize the actual energy portfolio has concentrated on molecular hydrogen (H_2) as a clean energy vector with high gravimetric energy density.[1–11] In this regard, water splitting has attracted a great deal of attention as a clean source of green hydrogen, but its large scale exploitation is restricted by the sluggish kinetics of the oxygen evolution reaction (OER), typically driven by precious metal-based electrocatalysts.[5,8,12–24] In order to properly tackle these issues, over the last years numerous efforts have been focused on the mastering of non-noble and efficient OER electrocatalysts,[3,6,25–27] capable of promoting O_2 evolution at low overpotentials.[15] Among the possible candidates, transition metal-based materials have drawn a considerable interest, owing to their variable electronic configurations and multiple oxidation states, ultimately yielding a favourable electrocatalytic activity.[1,15,16,19,20,27] In particular, nickel oxides and (oxy)-hydroxides, featuring enhanced reaction kinetics and improved structure/performance stability, are very valuable precious-metal-free catalysts for alkaline OER.[2,9,14,17,18,23,28,29] Especially, highly abundant and low-cost nickel(II) oxide has shown a great potential,[30–33] and various experimental and theoretical studies have been dedicated to the investigation of the pertaining structure–property interplay.[3,11,17,18,28,34–36] Nonetheless, since they still fall short of traditional noble metal-based ones,[7,12] various routes, including nanostructuring, functionalization, heterostructure formation, doping, and defect engineering have been proposed to boost their activity.[2,5–7,9,10,13,20–23,25,27,29,33] Nevertheless, the physical origin of NiO-based OER electrocatalysts activity at the atomic/nano-scale deserves further attention to promote their possible real-world end-uses.[16]

In this work, we propose as a proof-of-concept a combined route based on an original plasma processing and laser treatment to produce NiO-based electrocatalysts. Basing on our recent results,[37] the target process involves the initial plasma assisted-chemical vapor deposition (PA-CVD) of NiO nanostructures on conductive fluorine-doped tin oxide (FTO) glass substrates at 200, 300, and 400 °C (Fig. 1). The fabricated systems, whose features can be modulated as a function of growth temperature, are subsequently subjected to treatments using ultra-short laser pulses, in conjunction with a nanometric-resolution movement stage.[38,39] In this way, a laser-induced nanotexturization is achieved *via* the formation of peculiar surface structures. These self-organized patterns arise from the interference of the incident laser radiation with surface-scattered waves, resulting in energy deposition and material restructuring at the nanoscale. In fact, the ultra-short pulse duration enables electronic excitation and ablation processes to occur faster than thermal diffusion. As a result, the process

[a] *CNR-ICMATE and INSTM, Department of Chemical Sciences, Padova University, 35131 Padova, Italy. E-mail: davide.barreca@cnr.it*
[b] *CNR-ISM, Sez. Montelibretti, DiaTHEMA Lab, 00010 Montelibretti (RM), Italy*
[c] *CNR-ISM, Sez. Tito Scalo, 85050 Tito Scalo (PZ), Italy*
[d] *Department of Chemical Sciences, Padova University and INSTM, 35131 Padova, Italy*

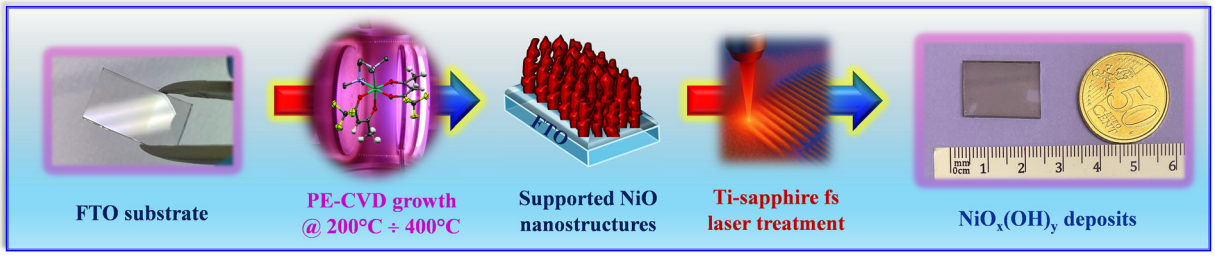

Fig. 1 Schematic representation of the strategy adopted in the present work for the fabrication and processing of NiO-based electrocatalysts.

yields functional nanostructures[40,41] characterized by a highly porous structure, an enhanced defect content, and a partial surface hydroxylation. As a matter of fact, the formation of a surface oxyhydroxide layer on NiO is reported to occur during OER, such species being the most active ones.[2,3,28,42,43] Additionally, the more hydrophilic catalyst surface facilitates electrolyte diffusion and favors removal of O_2 bubbles.[44] As a whole, the above laser-induced transformation beneficially impacts on the OER activities of the developed materials, that are well positioned in the overall panorama of Ni-based oxides/oxyhydroxides. Additional advantages of the proposed route are related to the elimination of hazardous chemicals/harsh temperature conditions and to the reduction of the synthetic steps required for material processing. As a consequence, the present procedure stands as an environmentally friendly alternative in the fabrication and mastering of advanced functional materials for sustainable energy applications.

Preliminary structural characterization by X-ray diffraction (XRD; Fig. S1, SI) evidenced the formation of cubic NiO as the sole crystalline phase in the target electrocatalysts. The recorded patterns featured a limited number of broad and relatively weak peaks, suggesting that the processed samples were formed by defective crystalline domains. Morphological analyses by field emission-scanning electron microscopy (FE-SEM, Fig. 2 and Fig. S2, S3, SI) revealed appreciable variations in comparison to the pristine specimens. In fact, laser-treated systems evidenced the formation of hierarchical structures, with elongated island-like features separated by deep grooves, resulting in an increased roughness and an enhanced material surface area. In particular, a more ordered structure was obtained for the 400 °C sample, dominated by longitudinal periodical grooves, whereas the ones fabricated at lower temperatures featured a certain degree of disorder, related to their more porous structure. Such a morphology can ensure optimal interaction with the reaction medium during OER functional tests. Cross-sectional micrographs (Fig. S3, SI) revealed a very good deposit adhesion to the FTO substrate and an average thickness of ≈80 nm for all the target specimens.

Chemical composition was investigated by X-ray photoelectron spectroscopy (XPS). It is worthwhile recalling that, in general, the analysis of Ni 2p signals is a challenging issue and a detailed assignment of the observed features is controversial,[45] being complicated by contributions of Ni 3d-O 2p related transitions that result in a complex satellite structure.[37] Beyond a detailed interpretation,[45–48] for all the present samples the Ni 2p photopeak shape was qualitatively similar (Fig. 3a). As regards the j = 3/2 spin–orbit contribution, the main difference relies on the intensity ratio between the two low binding energy (BE) components (1 and 2 in Table S1, SI). In spite of the complex spectral shape, this ratio can act as a qualitative indicator for the occurrence of Ni^{2+} and Ni^{3+},[49,50] the latter originating from O vacancies rather than from a subsidiary Ni_2O_3 phase.[45,51] In this regard, the co-presence of the above XPS bands 1 and 2 suggested the formation of an hydroxylated surface, resulting from the coexistence of $Ni(OH)_2$ and NiO(OH), that can be formulated as $NiO_x(OH)_y$. In particular, NiO(OH), containing Ni^{3+} centers (whose content can be indirectly estimated by the analysis of the O 1s signal (see Table S1, SI and pertaining comments),[49,50] can be formed even from $Ni(OH)_2$ according to the reaction:[43] $Ni(OH)_2 \rightleftharpoons NiO(OH) + H^+ + e^-$. Accordingly, O 1s signals (see Fig. 3b) resulted from the concurrence of different bands related not only to NiO, but also NiO(OH), $Ni(OH)_2$, and adsorbed water (compare Table S1, SI). For laser-treated samples, the hydroxylation degree was directly dependent on the adopted growth temperature, according to the order 400 °C < 300 °C < 200 °C

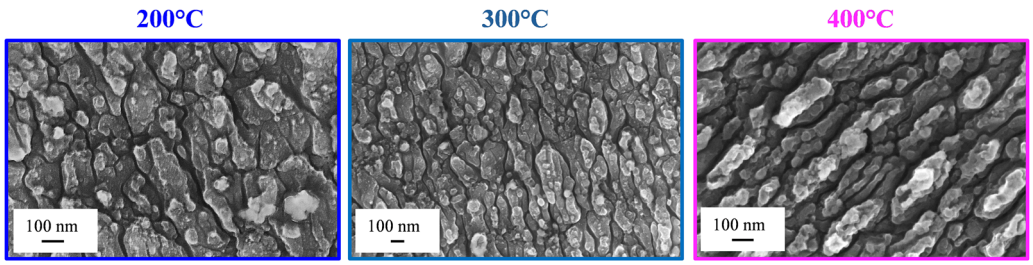

Fig. 2 Representative plane-view FE-SEM images for laser-treated samples grown at different temperatures.

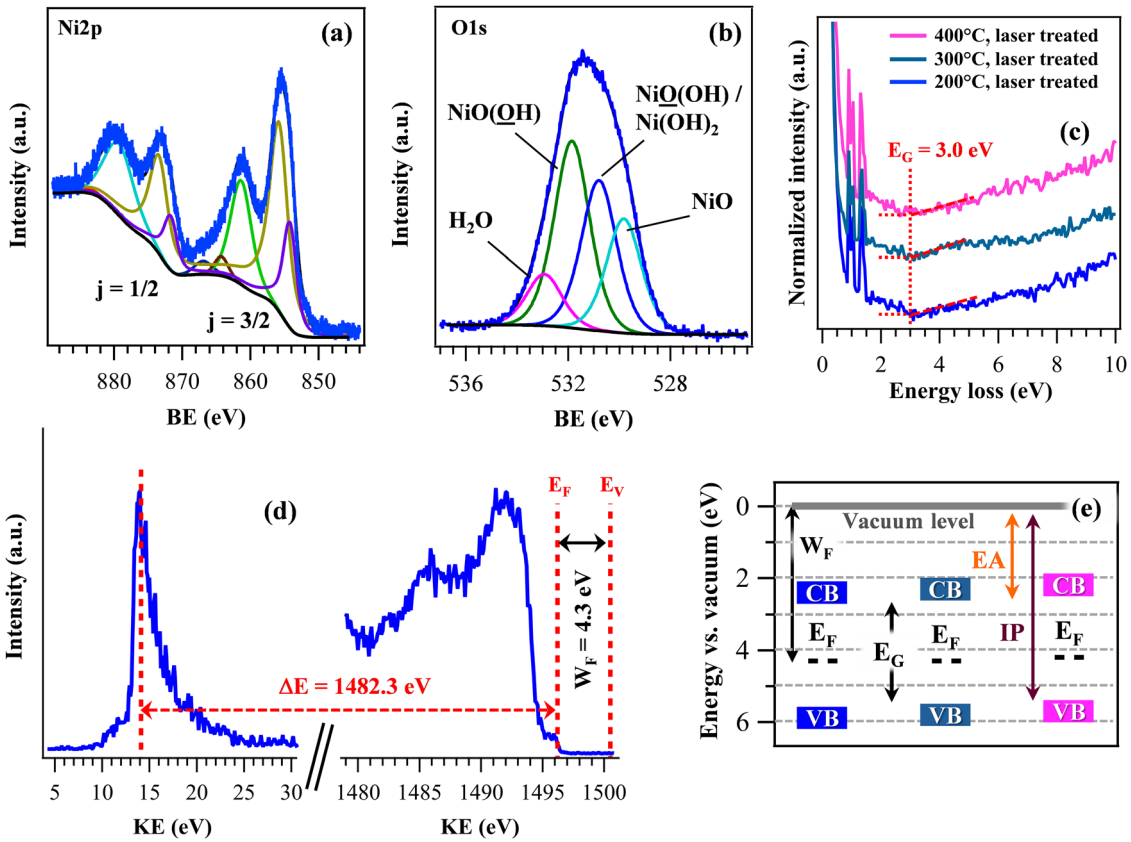

Fig. 3 Ni 2p (a) and O 1s (b) photopeaks for a laser-treated specimen grown at 200 °C. REELS spectra (c) and XPS VB with photoemission cutoff (d) after laser treatment. (e) Energy level positions for the different specimens (KE = kinetic energy; E_F = Fermi energy; E_V = vacuum level; W_F = work function; E_G = band gap; CB = conduction band; VB = valence band; EA = electron affinity; IP = ionization potential).

(Table S1, SI). As already mentioned, it is reasonable to argue that the laser action induces the breakdown of Ni–O bonds with formation of a very porous and O-deficient structure. As a consequence, upon atmospheric exposure during the treatment, chemisorption of water molecules on the defective NiO surface readily yields Ni–OH bonds formation.[46] It is yet worthwhile noticing that laser treatment is modifying only the outermost material regions, whereas the inner ones are characterized by the presence of NiO, as testified by XRD outcomes (see above).

Reflection electron energy loss spectroscopy (REELS, Fig. 3c) and XPS valence band analysis together with photoemission cutoff (Fig. 3d) provided analogous results, regardless of the adopted growth temperature. The band gap ($E_G \approx 3.0$ eV) and work function values ($W_F \approx 4.3$ eV) were similar for all samples[52] (see also Table S2, SI) and further supported the presence of a porous $Ni(OH)_2$ surface layer on the NiO deposit after laser treatment (NiO would feature a wider band gap of $\approx$3.6 eV). Altogether, the obtained data enabled us to construct the band scheme reported in Fig. 3e, indicating that laser treatment did not produce remarkable differences in the electronic structure of materials grown at different temperatures. On the other hand, the extensive presence of surface sites and defect states in laser-treated materials boosted their electrocatalytic activity (compare Fig. 4b–d and Fig. S4a, b, SI), as indicated not only by the systematic current density increase, but also by the lower onset potentials in comparison to the pristine electrocatalysts (see Fig. 4c and Table S3, SI). In fact, all the key performance indicators, encompassing overpotential values, Tafel slopes, and turnover frequency (TOF) values (Fig. 4e, f and Fig. S4c, d, SI) supported the general improvement brought about by laser processing. It can be argued that, during electrochemical testing, the $Ni(OH)_2$ surface layer undergoes the following oxidation reaction: $Ni(OH)_2 + OH^- \rightleftharpoons NiOOH + H_2O + e^-$, while the underlying NiO facilitates electron transport to the external circuit due to its higher conductivity. At the same time, NiO presence mechanically stabilizes the electrode structure, preventing volume expansion and phase degradation of $Ni(OH)_2$, while the latter enhances the electrochemically active area due to its high porosity. Thus, $Ni(OH)_2$/NiO coupling plays a fundamental role to explain the mechanism favoring the OER.

Remarkably, the electrocatalytic functional performances of the processed materials compare favorably with those reported so far for numerous mono- and bimetallic electrocatalysts based on Ni oxides and hydroxides prepared by conventional routes, as well as with those of various RuO_2 and IrO_2 systems, commonly considered as benchmark (Tables S3 and S4, SI). This comparison highlights the validity of the presently proposed processing route in boosting material functional

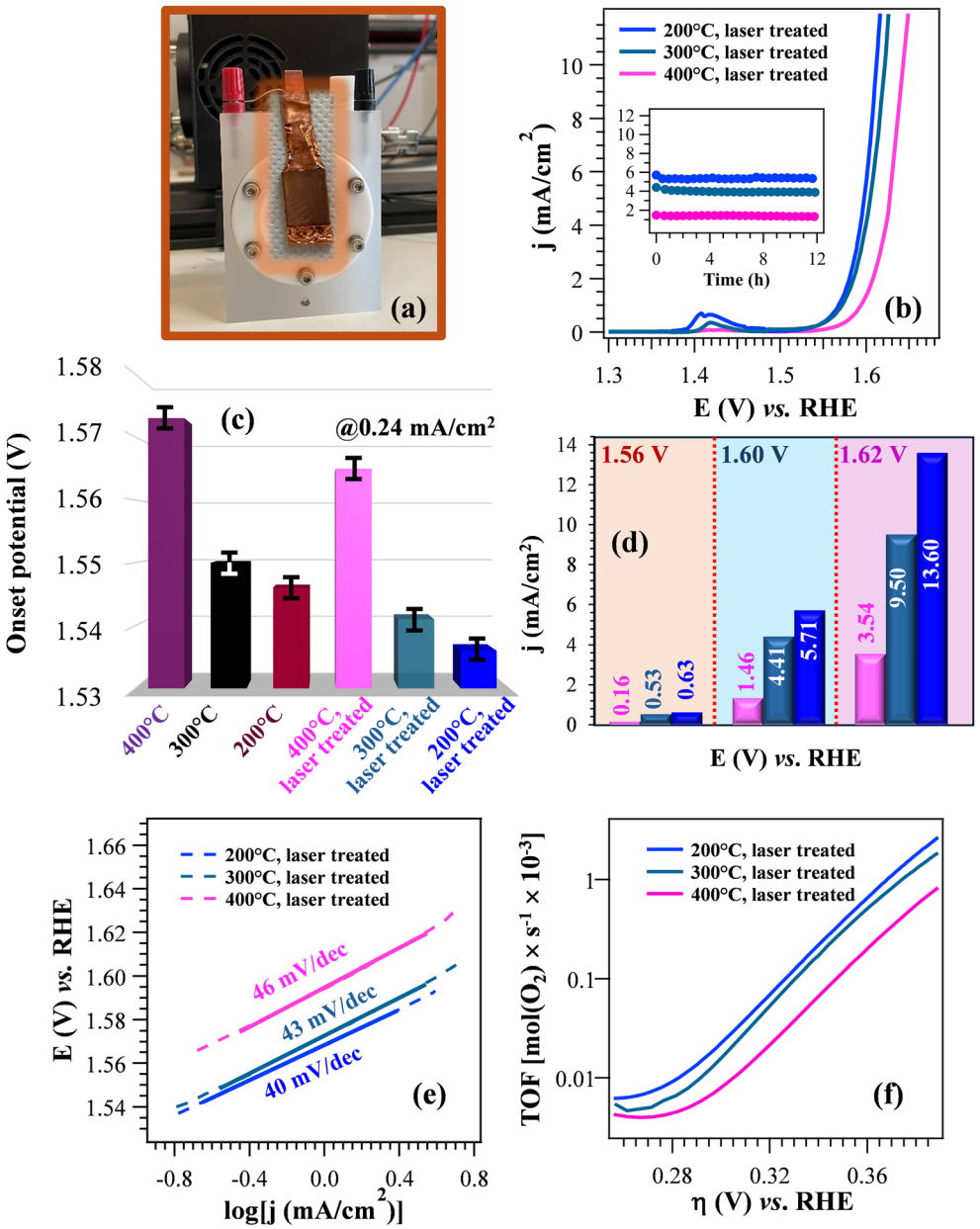

Fig. 4 (a) Digital image of the cell used for OER electrochemical tests. A photograph of a test sample after application of electrical contacts to prepare the working electrode is superimposed. (b) LSV traces for laser-treated specimens. Inset: chronoamperometric traces for the target specimens, recorded at 1.60 V *vs.* RHE. (c) Onset potentials for laser-treated and untreated specimens. (d) Current densities at different potential values for laser-treated samples. (e) Tafel slopes and (f) TOF *vs.* overpotential curves for laser-treated electrocatalysts. In (e), dashed and continuous lines correspond to experimental and fitting curves, respectively.

performances. The electrocatalytic activity increase of laser-treated electrocatalysts followed the order 400 °C < 300 °C < 200 °C, the same as in the pristine specimens, in line with the more open morphology obtained at lower growth temperatures (see Fig. S2, SI). The above reported XPS data showed that laser treatment resulted in a surface hydroxylation extent following the OER activity trend. In fact, a highly hydroxylated surface features an appreciable amount of NiO(OH), commonly considered as the catalytically active species. These results are also in agreement with the obtained integrated charges, proportional to the electrochemically active surface area (ECSA) values, estimated by integrating the cyclic voltammetry (CV) scans, showing the formation of NiO(OH) (Fig. S5, SI).[42] The obtained data amounted to 2.4, 2.1, and 1.1 mC for laser-treated NiO samples grown at 200, 300, and 400 °C, respectively. As an example, a charge of 2.4 mC corresponds to about 5.5×10^{16} active sites/cm^2, consistently with previous literature results.[27] Interestingly, the comparison of CV curves for laser-processed samples with the corresponding as-grown systems revealed that the NiO → NiO(OH) oxidation peak was significantly less intense and shifted at higher bias values in the latter case (Fig. S5, SI). Such findings indicate that laser

irradiation offers a versatile and controllable strategy to engineer the electrocatalytic properties of NiO surfaces.

In view of an eventual real-world utilization, an important parameter is the electrocatalyst service lifetime. In the present case, the very attractive performances of laser processed-electrocatalysts were accompanied by a remarkable stability, as evidenced by chronoamperometric tests (Fig. 4b, inset). Accordingly, *post operando* FE-SEM and XPS analyses (Fig. S6 and S7, SI) enabled to rule out appreciable morphological and compositional alterations upon prolonged testing.

In conclusion, the present study has reported on an original strategy for the fabrication and processing of NiO-based electrocatalysts for water oxidation. The developed approach involved the initial plasma-assisted fabrication of NiO-based nanomaterials, followed by a controllable laser treatment. The obtained results evidenced the formation of high area nanosystems, characterized by a partial NiO → $NiO_x(OH)_y$ surface conversion and features directly dependent on the adopted growth temperature. The corresponding OER activity showed an appreciable improvement, the best performances (obtained for the sample grown at 200 °C) corresponding to a Tafel slope of ≈40 mV × dec^{-1} and an overpotential (at 10 mA × cm^{-2}) of ≈380 mV. The activity of the developed electrocatalysts, coupled with their remarkable stability, underscores their attractiveness as viable materials for sustainable energy solutions. Thanks to the absence of toxic chemicals and of harsh *ex situ* treatments, and its relative simplicity, the present method overcomes various constraints of traditional synthesis techniques and adheres to sustainable chemistry principles.

The observed correlation between laser-induced modifications and the enhanced functional performances candidates this approach as a powerful tool for the design of cost-effective and eco-friendly OER electrocatalysts. In this regard, whereas preliminary studies evidenced that the developed NiO-based systems are inactive as cathodic (or bifunctional)[53,54] electrocatalysts toward the hydrogen evolution reaction (HER), their anodic performances will be further assessed in other technologically relevant processes, such as OER from seawater and urea oxidation reaction.[55,56] In addition, the developed processing route is potentially transferable to a variety of different substrates, ensuring also scalability and uniformity for the development of large-area electrodes, a valuable issue for an eventual implementation into commercial electrolyzers. The latter would require long-term electrochemical tests, even at higher current densities, to properly assess the actual material stability under operating conditions close to real-world ones.

Conflicts of interest

There are no conflicts to declare.

Data availability

The authors confirm that the data supporting the findings of the study are available within the article and the supplementary information (SI). Supplementary information is available. See DOI: https://doi.org/10.1039/d5ya00273g.

Acknowledgements

This work was financially supported by the National Research Council (Progetti di Ricerca @CNR-avviso 2020-ASSIST), Padova University (PDiSC#02BIRD2023-UNIPD RIGENERA, DOR 2023–2025), INSTM Consortium (TRI.25/013-CIMENTO), European Union-Next Generation EU, Mission 4 Component 1, PRIN 2022J9CEFM (SPEEDHY project; CUP B53D23015370006) and PRIN 2022474YE8 (SCI-TROPHY project; Next Generation EU – Bando PRIN 2022 – M4.C2.1.1). Dr Mattia Benedet, Dr Lorenzo Signorin and Dr Enrico Scattolin are gratefully acknowledged for skilful experimental support.

Notes and references

1 T. Kou, S. Wang, J. L. Hauser, M. Chen, S. R. J. Oliver, Y. Ye, J. Guo and Y. Li, *ACS Energy Lett.*, 2019, **4**, 622–628.
2 J. D. Michael, E. L. Demeter, S. M. Illes, Q. Fan, J. R. Boes and J. R. Kitchin, *J. Phys. Chem. C*, 2015, **119**, 11475–11481.
3 F. Basharat, U. A. Rana, M. Shahid and M. Serwar, *RSC Adv.*, 2015, **5**, 86713–86722.
4 L. Gouda, L. Sévery, T. Moehl, E. Mas-Marzá, P. Adams, F. Fabregat-Santiago and S. D. Tilley, *Green Chem.*, 2021, **23**, 8061–8068.
5 S. G. Jo, C.-S. Kim, S. J. Kim and J. W. Lee, *Nanomaterials*, 2021, **11**, 3379.
6 P. T. Babar, A. C. Lokhande, M. G. Gang, B. S. Pawar, S. M. Pawar and J. H. Kim, *J. Ind. Eng. Chem.*, 2018, **60**, 493–497.
7 R. K. Mishra, V. Kumar, G. J. Choi, J. W. Ryu, S. M. Mane, J. C. Shin and J. S. Gwag, *Mater. Lett.*, 2022, **324**, 132740.
8 N. Weidler, J. Schuch, F. Knaus, P. Stenner, S. Hoch, A. Maljusch, R. Schäfer, B. Kaiser and W. Jaegermann, *J. Phys. Chem. C*, 2017, **121**, 6455–6463.
9 Q. Dong, C. Sun, Z. Dai, X. Zang and X. Dong, *ChemCatChem*, 2016, **8**, 3484–3489.
10 A. QayoomMugheri, A. Tahira, U. Aftab, M. I. Abro, S. R. Chaudhry, L. Amaral and Z. H. Ibupoto, *Electrochim. Acta*, 2019, **306**, 9–17.
11 T. Yu, Q. Xu, L. Luo, C. Liu and S. Yin, *Chem. Eng. J.*, 2022, **430**, 133117.
12 H. Liu, R. Xiong, S. Ma, R. Wang, Z. Liu, T. Yao and B. Song, *Energy Adv.*, 2025, **4**, 55–83.
13 D. Rathore, A. Banerjee and S. Pande, *ACS Appl. Nano Mater.*, 2022, **5**, 2664–2677.
14 Y. Chen, K. Rui, J. Zhu, S. X. Dou and W. Sun, *Chem. – Eur. J.*, 2019, **25**, 703–713.
15 M. Lee, H.-S. Oh, M. K. Cho, J.-P. Ahn, Y. J. Hwang and B. K. Min, *Appl. Catal., B*, 2018, **233**, 130–135.
16 Q. He, Y. Wan, H. Jiang, Z. Pan, C. Wu, M. Wang, X. Wu, B. Ye, P. M. Ajayan and L. Song, *ACS Energy Lett.*, 2018, **3**, 1373–1380.

17 M. Gao, L. He, Z.-Y. Guo, Y.-R. Yuan and W.-W. Li, *ACS Appl. Mater. Interfaces*, 2020, **12**, 443–450.
18 X. Zhou, Z. Xia, Z. Zhang, Y. Ma and Y. Qu, *J. Mater. Chem. A*, 2014, **2**, 11799–11806.
19 O. Diaz-Morales, I. Ledezma-Yanez, M. T. M. Koper and F. Calle-Vallejo, *ACS Catal.*, 2015, **5**, 5380–5387.
20 J. P. Hughes, P. S. Adarakatti, S. J. Rowley-Neale and C. E. Banks, *RSC Adv.*, 2021, **11**, 14654–14664.
21 V. D. Silva, T. A. Simões, J. P. F. Grilo, E. S. Medeiros and D. A. Macedo, *J. Mater. Sci.*, 2020, **55**, 6648–6659.
22 Z. Qiu, Y. Ma, G. A. Niklasson and T. Edvinsson, *Physchem*, 2021, **1**, 69–81.
23 T. Zahra, K. S. Ahmad, C. Zequine, R. K. Gupta, A. Guy Thomas and M. Azad Malik, *Sustainable Energy Technol. Ass.*, 2020, **40**, 100753.
24 K. L. Nardi, N. Yang, C. F. Dickens, A. L. Strickler and S. F. Bent, *Adv. Energy Mater.*, 2015, **5**, 1500412.
25 A. Mondal, A. Paul, D. N. Srivastava and A. B. Panda, *Int. J. Hydrogen Energy*, 2018, **43**, 21665–21674.
26 N. Hussain, W. Yang, J. Dou, Y. Chen, Y. Qian and L. Xu, *J. Mater. Chem. A*, 2019, **7**, 9656–9664.
27 S. Cosentino, M. Urso, G. Torrisi, S. Battiato, F. Priolo, A. Terrasi and S. Mirabella, *Mater. Adv.*, 2020, **1**, 1971–1979.
28 C. Kuai, Y. Zhang, L. Han, H. L. Xin, C.-J. Sun, D. Nordlund, S. Qiao, X.-W. Du and F. Lin, *J. Mater. Chem. A*, 2020, **8**, 10747–10754.
29 M. Yang, H. Zhu, Y. Zheng, C. Zhang, G. Luo, Q. Xu, Q. Li, S. Zhang, T. Goto and R. Tu, *RSC Adv.*, 2022, **12**, 10496–10503.
30 L.-A. Stern and X. Hu, *Faraday Discuss.*, 2014, **176**, 363–379.
31 K. Fominykh, J. M. Feckl, J. Sicklinger, M. Döblinger, S. Böcklein, J. Ziegler, L. Peter, J. Rathousky, E.-W. Scheidt, T. Bein and D. Fattakhova-Rohlfing, *Adv. Funct. Mater.*, 2014, **24**, 3123–3129.
32 Z. Guo, X. Wang, Y. Gao and Z. Liu, *Dalton Trans.*, 2020, **49**, 1776–1784.
33 E. Arciga-Duran, Y. Meas, J. J. Pérez-Bueno, J. C. Ballesteros and G. Trejo, *Electrochim. Acta*, 2018, **268**, 49–58.
34 K. Hemmati, A. Kumar, A. R. Jadhav, O. Moradlou, A. Z. Moshfegh and H. Lee, *ACS Catal.*, 2023, **13**, 5516–5528.
35 Z. Qiu, Y. Ma and T. Edvinsson, *Nano Energy*, 2019, **66**, 104118.
36 E. Fois, C. Maccato, D. Barreca, C. Invernizzi and G. Tabacchi, *Dalton Trans.*, 2025, **54**, 2765–2775.
37 D. Barreca, E. Scattolin, C. Maccato, A. Gasparotto, L. Signorin, N. El Habra, A. Šuligoj, U. L. Štangar and G. A. Rizzi, *Chem. Commun.*, 2025, **61**, 2945–2948.
38 M. Mastellone, M. L. Pace, M. Curcio, N. Caggiano, A. De Bonis, R. Teghil, P. Dolce, D. Mollica, S. Orlando, A. Santagata, V. Serpente, A. Bellucci, M. Girolami, R. Polini and D. M. Trucchi, *Materials*, 2022, **15**, 1378.
39 A. Santagata, M. L. Pace, A. Bellucci, M. Mastellone, E. Bolli, V. Valentini, S. Orlando, E. Sani, S. Failla, D. Sciti and D. M. Trucchi, *Materials*, 2022, **15**, 8333.
40 J. Bonse and S. Gräf, *Laser Photonics Rev.*, 2020, **14**, 2000215.
41 J. Bonse, *Nanomaterials*, 2020, **10**, 1950.
42 R. Martínez-Hincapié, J. Wegner, M. U. Anwar, A. Raza-Khan, S. Franzka, S. Kleszczynski and V. Čolić, *Electrochim. Acta*, 2024, **476**, 143663.
43 H. Moreno Fernández, J. Gallenberger, C. Mempin, I. Khalek, M. Neumann, S. Lotfi, S. M. Kim, M. Li, C. Tian and J. P. Hofmann, *Electrochim. Acta*, 2024, **498**, 144626.
44 J. Ryu and D. W. Lee, *J. Mater. Chem. A*, 2024, **12**, 10012–10043.
45 G. Pagot, M. Benedet, C. Maccato, D. Barreca and V. Di Noto, *Surf. Sci. Spectra*, 2023, **30**, 024028.
46 A. R. Blume, W. Calvet, A. Ghafari, T. Mayer, A. Knop-Gericke and R. Schlögl, *Phys. Chem. Chem. Phys.*, 2023, **25**, 25552–25565.
47 A. F. Carley, S. D. Jackson, J. N. O'Shea and M. W. Roberts, *Surf. Sci.*, 1999, **440**, L868–L874.
48 M. A. van Veenendaal and G. A. Sawatzky, *Phys. Rev. Lett.*, 1993, **70**, 2459–2462.
49 A. P. Grosvenor, M. C. Biesinger, R. S. C. Smart and N. S. McIntyre, *Surf. Sci.*, 2006, **600**, 1771–1779.
50 C. Lyu, Y. Li, J. Cheng, Y. Yang, K. Wu, J. Wu, H. Wang, W.-M. Lau, Z. Tian, N. Wang and J. Zheng, *Small*, 2023, **19**, 2302055.
51 J. Li, L. Li, S. Wang, R. Li, C. Wang, J. Cai, W. Cheng, J. Li, G. Zou and Z. Lu, *Sol. Energy Mater. Sol. Cells*, 2024, **269**, 112734.
52 C. Park, J. Kim, K. Lee, K. Oh Suhk, J. Kang Hee and S. Park Nam, *Appl. Sci. Conver. Technol.*, 2015, **24**, 72–76.
53 S. Dev, S. Nagappan, S. Kundu and S. P. Mukherjee, *ACS Appl. Mater. Interfaces*, 2025, **17**, 15319–15332.
54 Y. Yuan, C. Zhang, X. Zhang, B. Jia, X. Zhang, G. Wu, J. Hao and P. Lu, *ACS Appl. Mater. Interfaces*, 2025, **17**, 12248–12260.
55 A. M. Shah, K. H. Modi, P. M. Pataniya, K. S. Joseph, S. Dabhi, G. R. Bhadu and C. K. Sumesh, *ACS Appl. Mater. Interfaces*, 2024, **16**, 11440–11452.
56 N. Trivedi, K. K. Joshi, S. Siraj, P. Sahatiya, V. Patel, C. K. Sumesh and P. M. Pataniya, *Int. J. Hydrogen Energy*, 2024, **49**, 1113–1122.